Article

# Macrophage-induced reduction of bacteriophage density limits the efficacy of in vivo pulmonary phage therapy

Sophia Zborowsky [1,11], Jérémy Seurat [2,3,11], Quentin Balacheff [1,4], Solène Ecomard [1,5,6], Céline Mulet[1], Chau Nguyen Ngoc Minh [1,6], Marie Titécat [7], Emma Evrard[1], Rogelio A. Rodriguez-Gonzalez[3,8], Jacopo Marchi[3,9], Joshua S. Weitz [2,3,9,10] ✉ & Laurent Debarbieux [1] ✉

The rise of antimicrobial resistance leads to renewed interest in evaluating phage therapy. In murine models highly effective treatment of acute pneumonia caused by *Pseudomonas aeruginosa* relies on the synergistic antibacterial activity of bacteriophages with neutrophils. Here, we show that depletion of alveolar macrophages (AM) shortens the survival of adult male mice without boosting the *P. aeruginosa* load in the lungs. Unexpectedly, upon bacteriophage treatment, pulmonary levels of *P. aeruginosa* are significantly lower in AM-depleted than in immunocompetent mice. To explore potential mechanisms underlying the benefit of AM-depletion in treated mice, we develop a mathematical model of bacteriophage, bacteria, and innate immune system dynamics. Simulations from the model fitted to data suggest that AM reduce bacteriophage density in the lungs. We experimentally confirm that the in vivo decay of bacteriophage is faster in immunocompetent compared to AM-depleted animals and that AM phagocytize therapeutic bacteriophage. These findings demonstrate the involvement of feedback between bacteriophage, bacteria, and the immune system in shaping the outcomes of phage therapy in clinical settings.

Antimicrobials resistance (AMR) is recognized as one of the major threats to global health in the 21st century[1–3] with worrisome projections of millions of deaths yearly at a global scale[4]. Amongst bacterial pathogens, the WHO has identified the need for solutions to treat prioritized threats posed by multidrug resistant (MDR) pathogens that cannot be treated by many commonly used antibiotics[3,5].

In response to the AMR crisis, there has been a resurgence of interest in phage therapy, *i.e.* the use of bacterial viruses (bacteriophages

or phages) to treat bacterial infections, as an alternative or as a supplement to antibiotics[6,7]. Pre-clinical studies in animal models have demonstrated the efficacy of phage therapy in the treatment of bacterial infections[6–8]. While large phase II clinical trials are still required to advance the broad deployment of phage therapy, a steadily increasing number of patients have access to compassionate treatments in both USA and Europe[9]. A recent retrospective analysis of such 100 patients have shown that their general health improved for more than 70%[10].

[1]Institut Pasteur, Université Paris Cité, CNRS UMR6047, Bacteriophage Bacterium Host, Paris, France. [2]Institut de Biologie, Ecole Normale Supérieure, Paris, France. [3]School of Biological Sciences, Georgia Institute of Technology, Atlanta, GA, USA. [4]CHU Felix Guyon, Service des maladies respiratoires, Saint Denis, France. [5]DGA, Paris, France. [6]Sorbonne Université, Collège Doctoral, Paris, France. [7]Université de Lille, INSERM, CHU Lille, U1286-INFINITE-Institute for Translational Research in Inflammation, Lille, France. [8]Interdisciplinary Graduate Program in Quantitative Biosciences, Georgia Institute of Technology, Atlanta, GA, USA. [9]Department of Biology, University of Maryland, College Park, MD, USA. [10]University of Maryland Institute for Health Computing, North Bethesda, MD, USA. [11]These authors contributed equally: Sophia Zborowsky, Jérémy Seurat. ✉e-mail: jsweitz@umd.edu; laurent.debarbieux@pasteur.fr

The killing efficacy of bacteria by phages relies on well-studied mechanisms of adsorption, injection, replication, assembly and lysis whose efficiencies are influenced by the in vivo environment (the infected body site). However, the role of the mammalian immune response induced by the pathogen during phage therapy remains uncertain and sometimes contradictory. Several studies performed with murine models of immunosuppression have shown that phage therapy is effective at treating neutropenic mice infected with *Staphylococcus aureus*[11] or pathogenic *Escherichia coli*[12], but is ineffective for *Pseudomonas aeruginosa*-infected animals[13,14]. The use of mathematical models has enabled a deeper understanding of these in vivo interactions[15–17]. For example, Roach et al. demonstrated that phage therapeutic-induced clearance of *P. aeruginosa* from the lungs requires synergistic action of phages with neutrophils[14], via a mechanism termed immunophage synergy. Another study combining data and mathematical modeling showed the efficacy of the immunophage synergy in treating *E. coli* pulmonary infections was dependent on the size of the bacterial inoculum[18]. The prominent role of neutrophils in the lungs contrast with their density as they represent about 2% of immune cells in this organ[19], in contrast to alveolar macrophages (AM), which account for 55% of immune cells in the lungs of healthy humans[20].

AM are the first line of cell-mediated defenses against microorganisms inhaled into the respiratory system as resident phagocytes[21,22]. AM are also the predominant immune cells present in the alveoli in homeostasis[22,23] and have several critical functions during infection, participating in clearance of pathogens and repair of the host tissue damages[24,25]. *P. aeruginosa* pneumonia initiates with the activation of AM through recognition of the LPS by TLR-4 and the flagellin by TLR-5, followed by the secretion of chemokines and cytokines that recruit neutrophils[26–28]. Nevertheless, studies using AM-depleted animals (different mouse strains and depletion levels) showed mixed outcomes leaving uncertainties about the role of AM in managing *P. aeruginosa*[29–31]. Furthermore, the direct interactions between AM and phages and their effect on phage therapy are poorly understood, particularly given that the innate immune system could have negative interactions with phage particles that can be phagocytized by neutrophils, monocytes, tissue macrophages and dendritic cells[32]. However, the response of phagocytizing cells to phage particles is not ubiquitous and some phages do not seem to elicit any interaction with macrophages[32,33].

Here, we sought to assess the role and interactions of AM in the clearance of *P. aeruginosa* during acute pneumonia and its treatment by phage. We combined an in vivo and mathematical modeling approach to conceptualize and experimentally test the interactions between pathogenic bacteria, therapeutic phage and the innate immune system (including macrophages and neutrophils). As we show, although AM depletion negatively impacts survival of mice given exposure to *P. aeruginosa* in the absence of phage therapy, the depletion of AM can have unexpected benefits to the efficacy of phage infection and lysis leading to reduced levels of *P. aeruginosa* in phage-treated animal hosts.

## Results

### Infection in alveolar macrophage-depleted mice

In previous studies, the virulent phage PAK_P1 (93 kb, *Pakpunavirus*) has been demonstrated to efficiently treat *P. aeruginosa* pneumonia caused by strain PAKlumi (allowing in vivo recording of bioluminescence)[14,34]. With the same phage and bacterium system we aimed to investigate the role of AM using an in vivo depletion approach relying on the intra-tracheal administration of clodronate in liposomes at a concentration known to cause macrophage apoptosis[21,35]. We found that 96 h after a single administration of clodronate the AM population decreases in median (min-max) by 98%

(95%-99%), while we did not observe an additional significant effect on lung nor blood neutrophils and dendritic cells (DCs) (Fig. 1A, Supplementary Figs. 1, 2).

We then compared the virulence of the *P. aeruginosa* strain PAKlumi in AM-depleted mice with control mice that received empty liposomes (EL). We found that 100% of AM-depleted mice had reached the compassionate end point within 24 h post-infection (p.i.), while it took over 48 h for the EL group (Fig. 1B). The dynamics of progression of the infection in the lungs was obtained through bioluminescent records over time for all animals showing that the average radiance between these two groups was not statistically different from 4 h to 20 h p.i. (Fig. 1C). Accordingly, in vivo *P. aeruginosa* growth rate comparisons based on the luminescence recordings between the EL and AM-depleted groups showed no significant differences (see source data file associated to Fig. 1C). Furthermore, lungs were recovered at compassionate end points to measure *P. aeruginosa* densities by colony forming units (CFUs) (Fig. 1D). We observed no significant difference in the CFUs levels between the two groups as suggested by the bioluminescent records at 22 h p.i. before sacrifice. Overall, AM depletion did not induce a significant effect on the in vivo growth rate of *P. aeruginosa* but AM depletion did have a significant and negative impact on survival. These results point towards the involvement of AM, as well as other immune cells including neutrophils, in the control and elimination of *P. aeruginosa*.

### Phage therapy rescues macrophage-depleted mice infected by *P. aeruginosa*

In order to assess the involvement of AM in the efficacy of phage treatment we administered a single dose of phage PAK_P1 at a multiplicity of infection (MOI) of 10 (related to the inoculum of strain PAKlumi) 2 h p.i., in both AM-depleted and EL mice. In EL mice the phage treatment increased the survival from 0% at 2.5 days to 67% at 8 days p.i., while in AM-depleted mice survival jumped from 0% at 24 h to 80% at 8 days p.i. (Fig. 1B). Therefore, the phage treatment increased significantly the survival in both AM-depleted ($p = 0.0058$) and EL mice ($p = 0.0016$) compared to the untreated groups. The survival rate at 8 days was not significantly different between the two phage-treated groups suggesting a similar efficacy of the antibacterial action of the phage. The bioluminescent recordings over time confirmed the rapid action of the phage as average bioluminescence values reached nearly the limit of quantification (LOQ) of 2000 p/s/cm²/sr equivalent to $5 \times 10^5$ CFU/mL at 8 h p.i. (i.e., 6 h post phage administration) (Fig. 1C) and were below the LOQ at 22 h p.i. in both phage-treated groups. Unexpectedly, the CFUs obtained from lungs of phage-treated animals sacrificed at 22 h p.i. showed that in the AM-depleted group no *P. aeruginosa* could be detected (limit of detection of $2.5 \times 10^2$ CFU/mL) in sharp contrast with the EL group that had levels around $10^5$ CFU/mL (Fig. 1D). This large difference in CFUs, although not detected from the luminescence data (values below the LOQ), indicates that the depletion of AM increases the clearance of bacteria by phage and suggests that AM may negatively impact phage therapy efficacy.

### Mathematical model of phage-immune feedback during phage therapy recapitulates in vivo dynamics in immunocompetent and AM-depleted mice

Building upon an immunophage synergy model[14] of in vivo phage therapy, we developed a mathematical model that includes the growth of bacteria, phage infection, lysis of susceptible bacteria, as well as the recruitment and clearance of bacteria by immune effector cells (neutrophils), which are themselves recruited by AM (Fig. 2 and Supplementary Methods for model specification including equations and parameterization). The parameterization of the in vivo phage therapy model was enabled by leveraging data obtained from

immunocompetent mice ($n = 44$) infected by strain PAKlumi (inoculum of $10^7$ CFU). Bioluminescence recordings were compared to equivalent time-point CFU measurements from plating to establish a correlation of luminescence with CFU data (adj-$R^2 = 0.71$, Supplementary Fig. 3A), which was further used to convert in vivo measurements for direct model-data comparison. Given the richness of these longitudinal data (Supplementary Fig. 3B), as well as individual phage loads (Supplementary Fig. 3C), immune cells data (Fig. 1A) and the observations previously described in the subsections and features of the immunophage synergy model[14], we set out to identify parameters that could recapitulate treatment dynamics in multiple conditions. Using normalized prediction distribution errors[36] from state-of-the-art practice in mixed effect modeling (Supplementary Fig. 4), we find that a common set of parameters in our in vivo phage therapy model can summarize observed time series dynamics in EL and AM-depleted mice both without or with phage while accounting for between-mouse variability (Fig. 3) and longitudinal data from all infected mice (Supplementary Fig. 5). We interpret model-data fits to mean that our baseline model can jointly explain the observed dynamics of bacteria, neutrophils, and AM in multiple conditions, insofar as phage rapidly proliferate in treated animals, even if there remains uncertainty in the extent to which there may be direct, negative interactions between components of the innate immune system and phage.

## Macrophage reduction of phage densities is essential to model in vivo data fits

To incorporate the faster progression of the infection observed in AM-depleted compared to EL mice, we tested two, non-exclusive hypotheses by varying the parameters of these processes: (i) phagocytosis of *P. aeruginosa* is eliminated in AM-depleted relative to EL mice; (ii) neutrophil recruitment is reduced in AM-depleted relative to EL mice (Fig. 2, Supplementary Methods: Eq. S1–S15). According to the model the difference in infection dynamics are better explained by a delay in recruitment of neutrophils rather than by reduced phagocytosis of bacteria in AM-depleted mice. The best model included a reduction of 50 % of the neutrophil recruitment rate in absence of AM. When adding the component of phagocytosis of *P. aeruginosa* by macrophages the model predictions did not align better with the observed infection dynamics than without phagocytosis (corrected Bayesian information criterion of 3359 vs. 3358, respectively); therefore, we removed AM phagocytosis of *P. aeruginosa* from the model. We incorporated the killing activity of the phage in our model to identify putative mechanisms to explain how phage therapy efficacy increased, albeit more so in AM-depleted than in EL mice. In the model framework, phage rapidly absorb and lyse bacteria. Bacterial growth is then controlled by a combination of phage and neutrophils that are progressively recruited in the lungs.
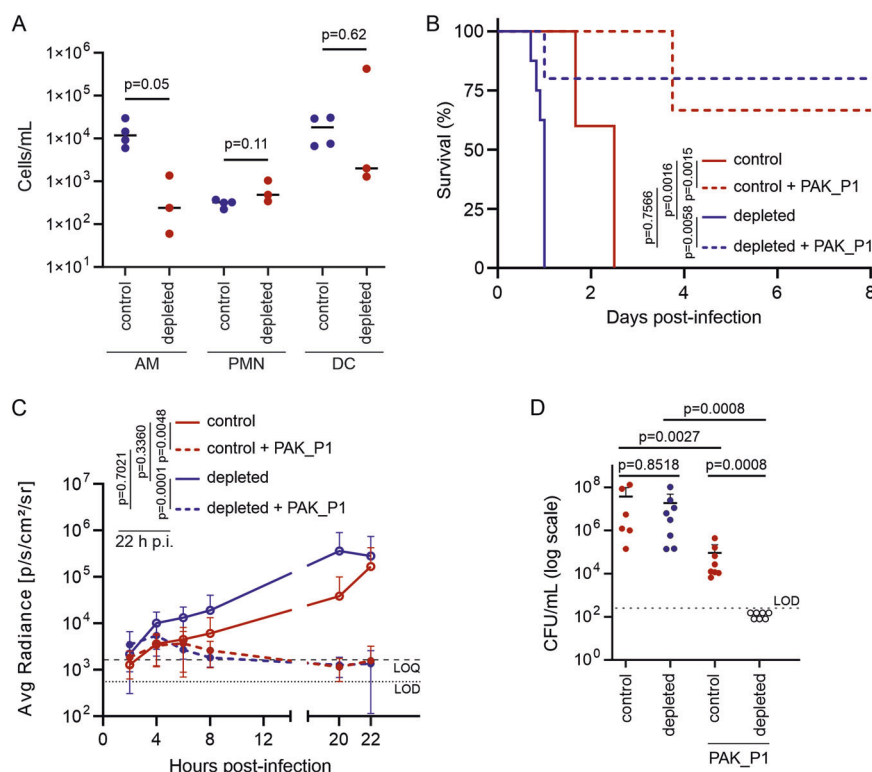


**Fig. 1 | Phage therapy in the macrophage depleted host. A** Flow cytometry analysis of bronco alveolar lavages (BAL) from mice that were given 96 h before clodronate liposomes (depleted) or empty liposomes (control) by intra-tracheal instillation ($n = 3$-4 each). Cell debris and doublets were first excluded based on CD45 staining. Among the CD45+ population Ly6G+ was used to gate PMN, in the Ly6G- population, the CD11b- correspond to dendritic cells (DC) and alveoli macrophage (AM). The DCs were gated as F4/80- and CD11c+ low while the AM as F4/80+ and CD11c+ high (*p* value from Mann-Whitney U test two tailed, are indicated). **B** Survival of acute respiratory infection caused by *P. aeruginosa* ($5 \times 10^6$ CFU of strain PAKlumi) of AM-depleted mice (clodronate, $n = 8$) and control mice ($n = 5$) was significantly different ($p = 0.0015$ Mantel-Cox log rank test) in absence of phage treatment (full lines). With phage PAK_P1 ($5 \times 10^7$ PFU) administered intranasally at 2 h p.i. (dashed lines) in AM-depleted ($n = 5$) and control (EL) ($n = 6$) mice, phage

treatment significantly improved their survival ($p = 0.0058$ and 0.0015, Mantel-Cox log rank test, for AM-depleted and control mice, respectively). Data were assembled from 5 independent experiments. **C** The colonization kinetics of the bioluminescent strain PAKlumi in the lungs is plotted as mean radiance (p/s/cm²/sr) over time with error bars representing SD. Groups of mice were infected and treated as in panel (**B**) with control ($n = 6$), AM-depleted ($n = 8$), phage-treated control ($n = 9$) and phage treated AM-depleted ($n = 13$). Statistical analysis (two-tailed Mann–Whitney U test) is indicated for the time point 22 h p.i. LOQ, limit of quantification. LOD, limit of detection. Data were assembled from 6 independent experiments. **D** Bacterial counts (CFUs in log scale) from lung homogenates taken from mice (same animals as in panel **C**) 22 h post infection. LOD limit of detection (*p* values from two-tailed Mann–Whitney U test are displayed). Data were assembled from 5 independent experiments.
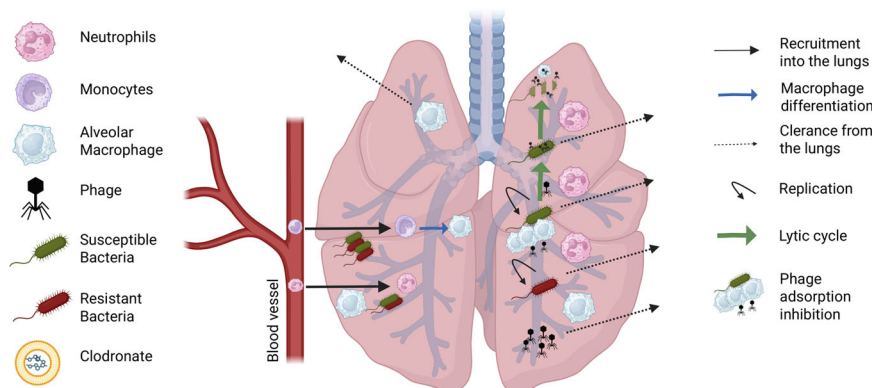
**Fig. 2 | Schematic model of bacteria-phage-macrophage-neutrophils interaction in the lungs.** An immune cell close to the arrow represents its impact on the corresponding process. Created in BioRender.com. A full list of equations and parameterization are found in Supplementary Methods.
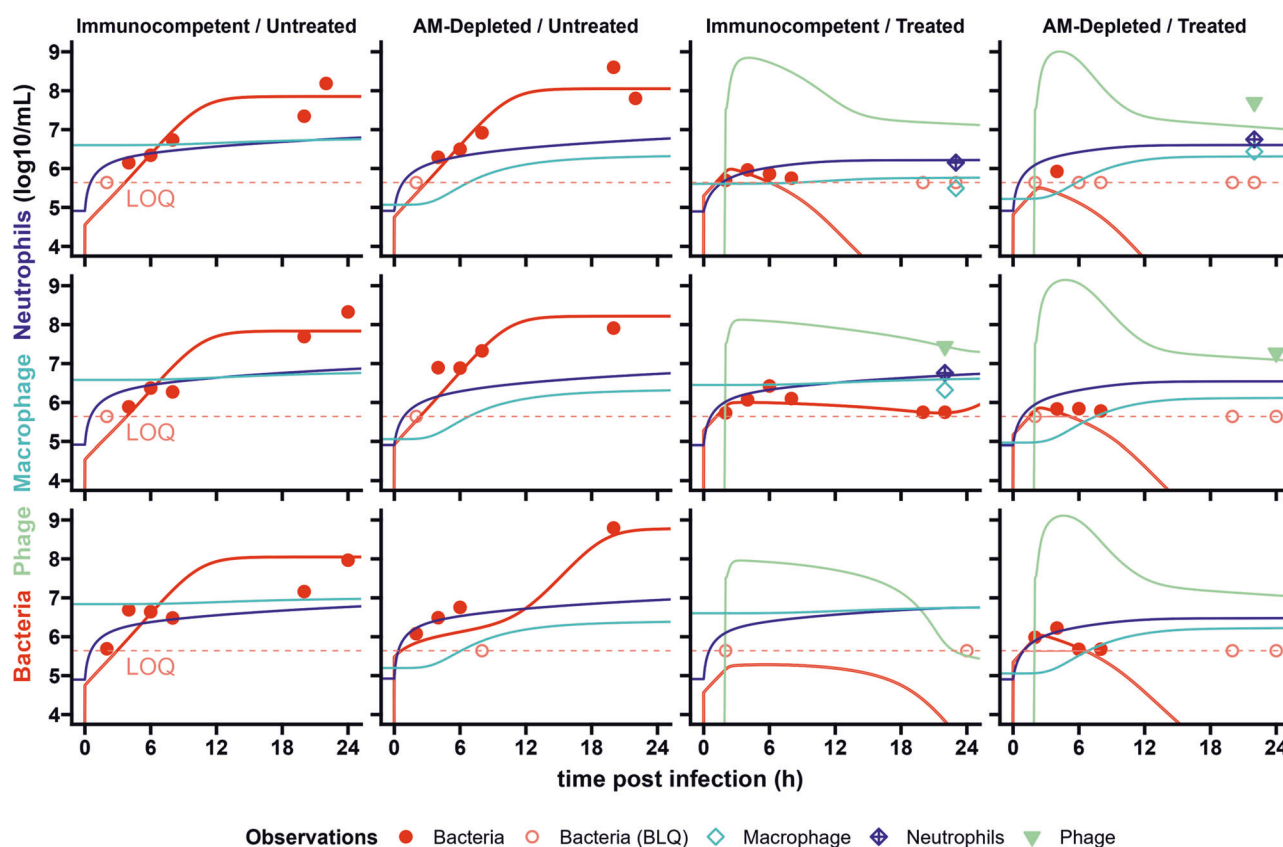


**Fig. 3 | Model of bacteria-phage-macrophage-neutrophils interaction in the lungs.** Individual model predictions and data for 3 mice from each group ranked in columns with corresponding headers. Bacteria are in red, phage in green, alveolar macrophage (AM) in light blue, and lung neutrophils in dark blue. Lines are model-based individual dynamics, dots are bacterial densities, triangles are phage concentrations, crossed squares are lung neutrophils and squares are AM. The light red horizontal dashed lines represent the limit of quantification (LOQ) for bacterial density (LOQ = 5.6 $\log_{10}$ CFUeq/mL), light red circles crossed by this line at their center are below the limit of quantification (BLQ) of bacterial density and light red lines are BLQ of bacterial load model-based predictions (i.e., the discrepancy between data and model cannot be evaluated from this plot in case of BLQ data).

We next hypothesized that the reduced clearance of *P. aeruginosa* in the lungs of EL mice was caused by the clearance of phage mediated by AM—if so, this would imply that fewer phage were available to infect and lyse *P. aeruginosa*, as observed 22 h p.i. (Supplementary Fig. 3C). We used the mathematical model to estimate the AM-mediated decay rate of phages, assuming no other interaction between phage and macrophage. We compared CFU densities in the lung to predicted median bacterial dynamics from a mathematical model incorporating phage kinetics in an in vivo context. This model included dynamics of pulmonary bacteria, phage, AM and neutrophils while assuming various AM-mediated decay rates. We found that a decay rate of phage PAK_P1 around 8 times higher in EL compared to AM-depleted animals would explain the difference in the CFU data between EL (Fig. 4A) and AM-depleted (Fig. 4B) mice. Indeed, in EL mice every lower decay rate resulted in predicting lower bacterial loads compared to observed data, whereas a higher decay rate led to a late emergence of resistant bacteria, which is not compatible with the radiance data (Fig. 1B) and survival (Fig. 1C). In AM-depleted mice, due to the rapid adsorption and
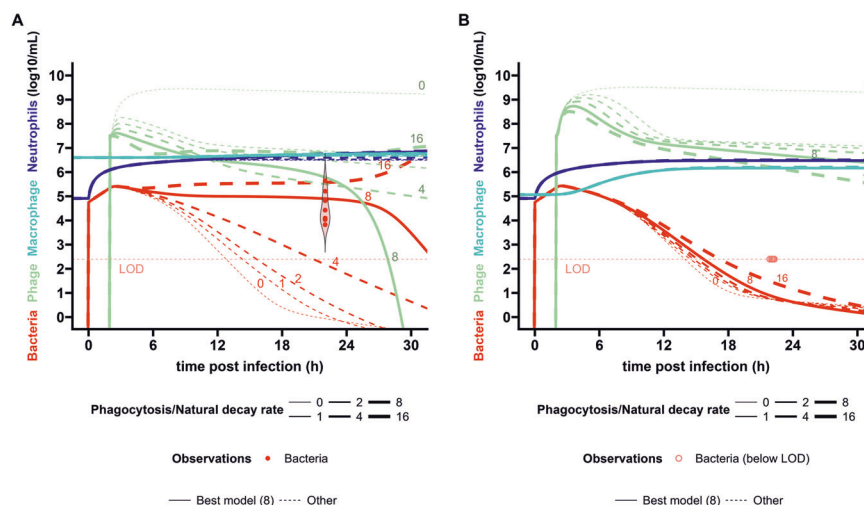
**Fig. 4 | Median dynamics with various AM-mediated phage decay rate parameter values after infection and phage treatment.** Dynamics of bacteria (red), phage (green), alveolar macrophage (AM, light blue), and lung neutrophils (dark blue) based on the model and its median parameters (Fig. 2A, Supplementary Methods), assuming no interaction between macrophages and phage except AM-mediated decay. Each panel corresponds to the different mice groups according to their immune status: **A** immunocompetent control (i.e., empty liposome), **B** AM-depleted (clodronate). Line widths increase depending on the AM-mediated decay rate (multiplied by the macrophage density): 0,1,2,4,8 and 16 times the phage decay in absence of AM, from the thinnest to the widest line. This number is also indicated above the corresponding median bacteria and phage dynamics. The AM-mediated/natural decay rate value leading to the best model (i.e., 8) is represented by solid lines, while the others are represented by dotted lines. The violin and the dots represent the distribution and values of observed CFUs. The limit of detection (LOD) for CFUs is represented by the light red horizontal dashed line (LOD = 2.4 $\log_{10}$ CFU/mL). For AM-depletion, all the observations were below the LOD.

lytic parameters of the phage, all the AM-mediated decay rate values between 1 and 16 times the natural decay (i.e. not AM-mediated decay) rate were compatible with the non-detectable bacteria at 22 h p.i. (Fig. 4B). Hence, the mathematical model suggests that AM could reduce phage densities in vivo which would have deleterious effects on the efficacy of phage therapy in immunocompetent murine hosts but, in contrast, synergistic effects in AM-depleted murine hosts.

**Phagocytosis is involved in phage decay**

In order to test if AM reduced phage concentration in the lungs, we administered a single dose of phage PAK_P1 to AM-depleted and EL mice and sacrificed animals over time to assess phage decay rates in vivo. We found that the levels of PFUs were significantly lower in the EL compared to the AM-depleted mice across all time points (Fig. 5A). Performing nonlinear regressions, the phage decay rate was significantly 3 times lower (3.1, CI$_{95}$: [2.9, 3.2], $p < 0.0001$) in the depleted compared to the EL groups (0.023 [0.016,0.029] h$^{-1}$ vs. 0.069 [0.067, 0.071] h$^{-1}$), which corresponds to elimination half-lives of 30 h and 10 h, respectively. Moving one step further we quantified by qPCR the amount of phage DNA recovered from AM sorted (CD45, CD11c and Singlec-F positive cells) from bronco-alveolar lavages (BAL) of lungs of mice exposed to either PBS or PAK_P1. The five mice that were administered intranasally phage PAK_P1 had a mean number of phage DNA copies per AM ranging from 2.6 to 6.0 while no phage DNA was detected in PBS-treated mice (Fig. 5B). Altogether, these data suggest that phage are being removed from the lungs by AM at a rate which is consistent with a previous study evaluating phage decay in immunocompetent hosts (0.07 h$^{-1}$)[14].

Next, we performed in vitro assays by first incubating phage PAK_P1 with murine macrophage J774 cell line at three phage:cell ratios during 24 h. We observed no significant differences in phage titers (Supplementary Fig. 6A). Second, we incubated phage PAK_P1 with AM collected from uninfected mice in the absence and presence of cytochalasin B, a drug known to inhibit phagocytosis. We observed a significant increase of phage-associated fluorescent signals in AM in the absence of cytochalasin B compared to its presence at times 3 h and 5 h

post-incubation demonstrating a significant phagocytosis of phages by AM (Fig. 5C, D, Supplementary Fig. 6B, C). These data suggest that either macrophage J774 cell line are unable to phagocytose phage in contrast to AM or, more likely, that phagocytosis of phages was not detectable by direct plating.

However, the mathematical model predicts that the accelerated decay rate of phage is not high enough to explain the 3-log difference in CFUs observed at 22 h p.i. between these EL and AM-depleted mice (Fig. 1D), suggesting the presence of additional inhibitory mechanisms beyond phagocytosis. Macrophages have been shown to "cloak" areas of injury or infection in order to reduce neutrophils recruitment and sequential neutrophil-mediated inflammatory damages[37,38]. Macrophage that block access to bacteria might also reduce contact by phage, reducing adsorption. By setting values for natural phage decline and AM-mediated decay rate to the observed values, we investigated a range of AM-induced reduction of phage adsorption within our mathematical model. In EL mice, the combination of the removal of phages at a rate of 0.069 h$^{-1}$ with a reduction of phage adsorption by 30% generated *P. aeruginosa* clearance rates corresponding to the experimental CFUs in this group whereas a lower value such as 15% led to faster clearance than observed and a higher value such as 60% led to bacterial control (Fig. 5E). In AM-depleted, the different adsorption inhibition values, including 30%, all recapitulate the bacterial clearance at 22 h p.i., since the low density of AM was insufficient to inhibit phage adsorption in the first 10 h p.i., allowing phages to multiply and hence rapidly clear bacteria (Fig. 5F). Interestingly, the combination of the two AM-phage processes (phage decay and adsorption inhibition) could explain the small difference (about 1 log) of phage density between EL and AM-depleted mice (Supplementary Fig. 3C).

Overall, the negative effects of AM on phage efficacy result in the median bacterial load stabilizing during the 18 h following phage administration in the EL mice (Fig. 5E) versus 4 h in the AM-depleted animals (Fig. 5F). This negative effect of AM on phage concentration is counterbalanced by the infection parameters of phage PAK_P1 (rapid adsorption rate of 1.2 10$^{-7}$ mL/PFU/h, lytic cycle of 20 min and
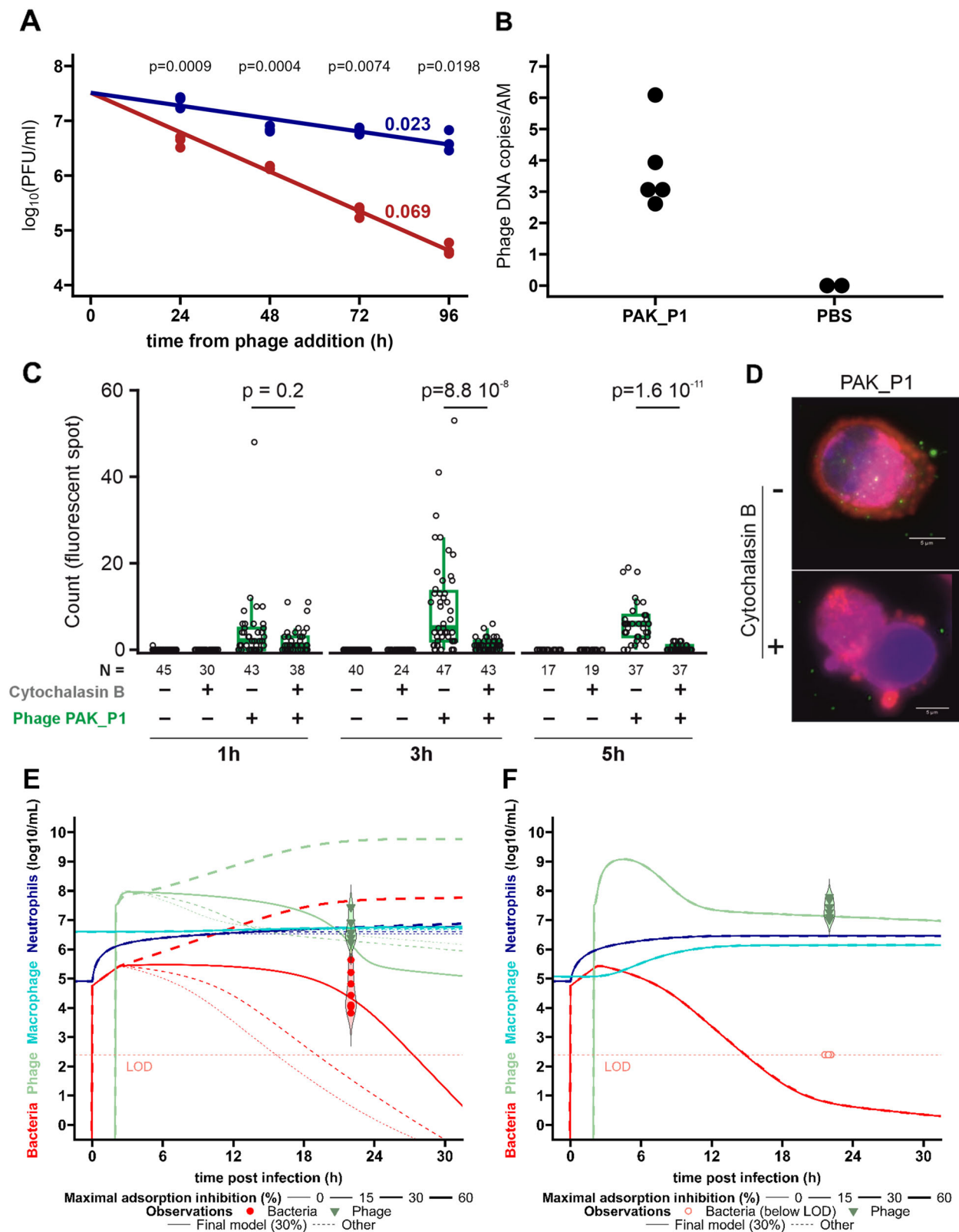
burst size of 100[14]), leading to decreasing bacterial load. From our model-based simulations accounting for inter-individual variability, differences were noted between the EL and the AM-depleted phage-treated groups (Fig. 6). Indeed, in the EL group, our model predicts a bacterial rebound of over $10^7$/mL for at least 25% of individuals 30 h post-infection, whereas in the AM-depleted group, over 75% of individuals had bacterial load below $10^4$/mL. Notably, the antagonistic

interactions between AM and phage could result in loss of bacterial infection control, depending on the phage dose. Our model predicts a possible rebound in bacterial load at MOI 0.1, i.e., with a dose 100 times lower than that used in our study. For AM-depleted individuals, the decline in bacterial load becomes slower as the phage dose decreases, without showing a rebound even at MOI 0.01 (Supplementary Fig. 7).

**Fig. 5 | AM-associated phage decay and adsorption inhibition assumption.**
**A** Uninfected mice were given clodronate (blue) or EL (red) by intra-tracheal
instillation (n = 3–4 each) 4 days prior phage PAK_P1 (5 × 10⁷ PFU) at t = 0 h. Lungs
were collected and homogenized at indicated time points. Data fitted using a
monoexponential decay model with decay rate values indicated (p values, two-
tailed Mann–Whitney U test, are indicated). **B** Uninfected mice received intranasally
PBS (n = 2) or phage PAK_P1 (5 × 10⁷ PFU) (n = 6) at t = 0 h and broncho alveolar
lavage was performed 4 h post-administration to sort and count AM and quantify
phage DNA by qPCR. **C** Counts of phage-associated fluorescent signals in individual
AM collected from uninfected mice and incubated without (control) or with phage
PAK_P1 in absence or presence of cytochalasin B (N = number of AM observed for
each condition). Boxplots display median (center line), first and third quartiles (box
limits), and whiskers extending to 1.5×IQR from the quartiles (p values, two-tailed
Mann–Whitney U test, are indicated). **D** Representative images from AM incubated

with phage PAK_P1 in presence or absence of cytochalasin B. Median dynamics with
various adsorption inhibition parameter values after infection and phage treatment
for (**E**) immunocompetent control (i.e. EL) and **F** AM-depleted mice. Dynamics of
bacteria (red), phage (green), alveolar macrophage (AM, light blue), and lung
neutrophils (dark blue) based on the model and its median parameters (Fig. 2A,
Supplementary Methods), assuming phagocytosis rate value from the inference of
the data of Fig. 4A. Line widths increase depending on the maximal adsorption
inhibition by AM: 0%, 15%, 30% and 60%, from the thinnest to the widest line. The
maximal adsorption inhibition value leading to the best model (i.e., 30%) is
represented by solid lines, while the others are represented by dotted lines. The
violin and dots represent the distribution and values of observations: CFUs in red
and PFUs in green. The limit of detection (LOD) for CFUs is represented by the light
red horizontal dashed line (LOD = 2.4 log₁₀ CFU/mL) For AM-depletion, all the
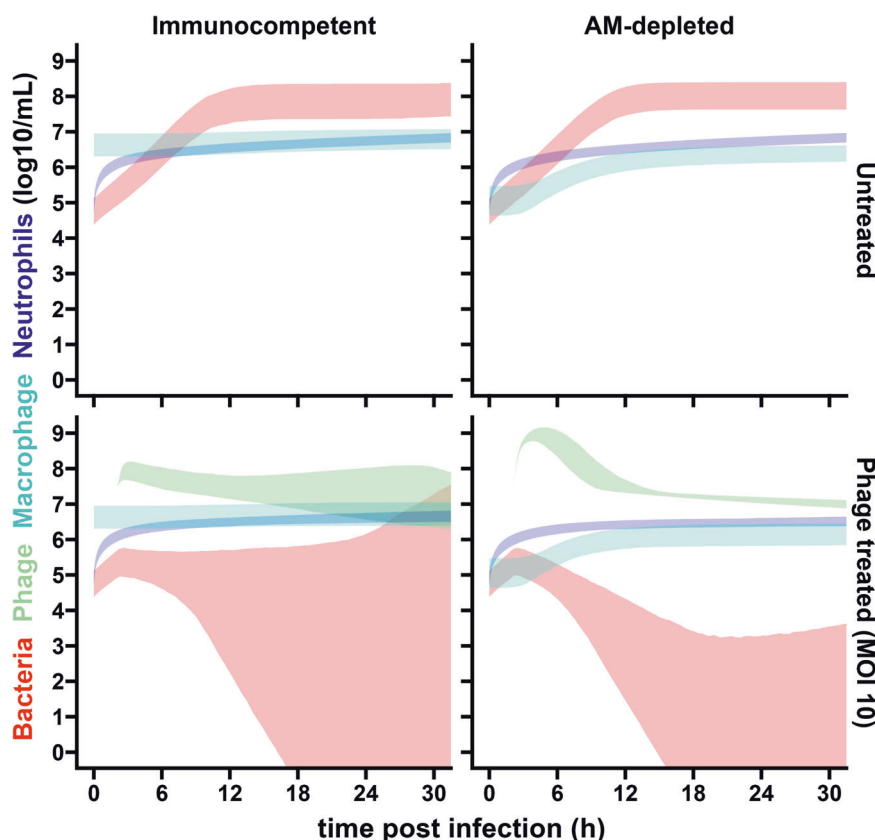observations were below the LOD.



**Fig. 6 | Inter-individual variability in the dynamics of bacteria, phage, alveolar
macrophage and lung neutrophils.** Based on the model (Fig. 2) and its median
and variability parameters (Supplementary Methods), simulations for 1000

individuals in each group are shown by areas covering interquartile interval (Q1-
Q3). Each panel corresponds to the different mice groups according to their
immune status and phage treatment.

## Discussion

In this study we examined the role of alveolar macrophage (AM) during
*P. aeruginosa* infection and treatment with phage leading to two cen-
tral conclusions. First, based on survival analysis we infer that AM are a
necessary immune component for survival of mice to *P. aeruginosa*
infection. Even though the initial progression of *P. aeruginosa* infection
is faster in the absence of AM – a feature which can be explained by the
delayed recruitment of AM-induced neutrophils into the lungs – the
bacterial load is not significantly different at the compassionate end
point. Thus, we concluded that the reduced survival in the absence of
macrophages is not related to the lack of phagocytosis of *P. aeruginosa*
by AM. Second, we found that phage therapy was curative in both
immunocompetent and AM-depleted mice given luminescence below
the LOQ before sacrifice and survival at 8 days above 60% in both
groups. Moreover, CFU levels recovered in the lungs of AM-depleted

mice treated with phage were at least four orders of magnitude lower
than that in immunocompetent mice. This difference between the two
groups could be detected only from CFU counts because the radiance
was below the LOQ in the two groups. This difference also implies that
AM directly reduce phage-induced clearance of *P. aeruginosa* in vivo.
Via mathematical modeling and direct in vivo experiments, we suggest
that macrophage-induced reduction of phage densities includes pha-
gocytosis and other mechanisms.

Macrophages are typically classified into two functional pheno-
types: pro-inflammatory M1 macrophages and anti-inflammatory M2
macrophages[25,39]. While M1 macrophages promote the inflammatory
response aimed at clearance of the pathogen, including phagocytosis
and recruitment of other cell types[24,25,39,40], the M2 macrophages par-
ticipates in resolution of the infection, tissue repair and return to
homeostasis[24,40,41]. Given that at 22 h p.i. the AM-depleted mice had the

same bacterial load as the immunocompetent mice, we hypothesize that the observed difference in survival between these two groups of mice is related to the lack of M2 activity, which would need further experiments beyond the scope of this study. Nevertheless, prior AM depletion studies reach different conclusions on the involvement of AMs in the survival of *P. aeruginosa* infected mice[29–31]. These differences may arise given that immune response varies depending on the bacterial strain and initial inoculum used in these studies. We identify the study by Cheung et al.[30] as the closest in terms of mouse line (BALB/c), AM depletion method and bacterial inoculum (different strain of *P. aeruginosa* however). Similar to the present findings, these authors observed no difference in CFUs in the lungs at 24 h p.i. between the AM-depleted and control groups, however the AM-depleted animals did not reach compassionate end points at 24 h p.i. The key difference is the level of AM depletion that reached 65% in their study compared to 95% in our study. This could account for the discrepancies in survival if we consider that the remaining population (35%) of AM is sufficient to recapitulate a WT phenotype.

In contrast to the contribution of AM in promoting efficient *P. aeruginosa* clearance from the lungs, we found that treatment with phage was more efficient at clearing infection in AM-depleted than in immunocompetent mice with significant lower levels of *P. aeruginosa*. Guided by a mathematical model, we discovered that phage decay in vivo was three times faster in immunocompetent compared to AM-depleted mice. This gap strongly points to macrophages involvement in active removal of phages from the lungs, by phagocytosis and/or other processes. There is prior evidence for phage phagocytosis by macrophages, which comes mostly from in vitro observations, where T2 phage was found to be internalized by rabbit macrophages and peritoneal neutrophils[42] and T4 phage was found inside rat dendritic cells[43] as well as inside murine macrophages[44]. Interestingly, we found no significant in vitro phagocytosis by macrophages using the J774 macrophage cell line. However, this line originates from reticulum cell sarcoma[45] and not from alveoli macrophages. Here, we showed AM were able to internalize phage PAK_P1 by phagocytosis. This emphasizes that different macrophages will not necessarily respond similarly to the same stimuli. According to our mathematical model, phage decay by AM was not enough to account for the differences in CFUs and PFUs found in the lungs at end points and we suggested that an additional effect of adsorption inhibition could provide an explanation. These interactions require further investigation in order to test if AM digest phage particles and if their presence reduces adsorption rates due to spatial interference, e.g., "cloaking" of bacterial colonization sites. More generally, mathematical model predictions remained robust to parameter variation even insofar as a subset of assumptions and parameter values in the mathematical model could not yet be verified experimentally in this study; efforts to do so must also account for ethical considerations involved with sacrificing a much larger number of animals.

Integrating AM-induced reduction of phage densities and adsorption in a mathematical model of in vivo phage therapy led to bacteria, phage, and immune system population dynamics consistent with in vivo data from immunocompetent and AM-depleted mice. However, our study comes with caveats. We did not address phage resistance during these experiments as we did not observe a rebound in the bacterial population in phage treated groups, which is usually associated with the growth of phage resistant bacteria. However, we did incorporate resistance to phage in our mathematical model as the bacterial rebound is associated with growth of a phage-resistant bacterial population. Assumptions about phage resistance rates in the model are derived from Roach et al.[14]. Hence, although we interpret the antagonistic impact of AM on phage induced lysis of *P. aeruginosa*, we recognize that evolutionary dynamics may further complicate these tripartite interactions[17]. Moreover, our model does not directly include the potential role of macrophages in murine host survival. We

hypothesize that macrophage mitigate against the accumulation of damages to the tissues which can lead to the rapid decline in the health of the animal. The hypothesis that M2 macrophage are necessary for survival of *P. aeruginosa* infection requires further investigations by assessment of tissue damages for example. In the long term, indicators of tissue damages should be integrated into mathematical models to better represent the role of macrophages during infection by *P. aeruginosa* and their impact on host health and survival.

In conclusion, we have found evidence for an antagonistic interaction between phages and macrophages during phage therapy. Phages are removed faster from the lungs by AM, which potentially lower phage adsorption to bacteria as well; together these mechanisms reduce the efficacy of phage therapy in immunocompetent relative to macrophage depleted murine hosts. Since prior evidence shows that not all phages are recognized and phagocytized by the immune system, our findings suggest that selection of therapeutic phage candidates, whether as single strain or as cocktails should take into account the response of the immune system – including both neutrophils and macrophages. More broadly, identifying inclusion criteria is essential to identify subpopulations of individuals who may be responsive to given therapies – including phage therapy. The finding here, building upon prior work on the key synergistic roles of neutrophils, can help guide follow-up studies to identify actionable criteria for phage therapy use in the context of personalized medicine.

## Methods
### Animals and ethics
This research complies with all relevant ethical regulations. BALB/c mice (nine to eleven weeks old purchased from Charles River) were housed in a pathogen-free animal facility in accordance with Institut Pasteur guidelines and European recommendations. Food and drinking water were provided *ad libitum*. Protocols were approved by the veterinary staff of the Institut Pasteur animal facility (Ref.#18.271), the National Ethics Committee (APAFIS#26874-2020081309052574 v1) and the Georgia Institute of Technology IACUC.

### Bacteria and phage
We used the bioluminescent *P. aeruginosa* strain PAKlumi that constitutively expresses the *luxCDABE* operon from *Photorhabdus luminescens*[46]. PAKlumi was grown in Lennox Broth (LB), at 37 °C with shaking at 180 rpm.

Phage PAK_P1 lysates were propagated on PAKlumi as previously described[47]. PAK-P1 was added to mid-log culture of PAKlumi at a multiplicity of infection (MOI) of 0.001. The infected culture was kept at 37 °C with shaking until lysis occured. The culture was centrifuged (7000 rpm, 10 min, 4 °C) and the supernatant filtered (0.2 μm) and then concentrated in Phosphate Buffered Saline (PBS) (Sigma) by ultrafiltration (Vivaflow 200™; Sartorius). The lysates were purified by cesium chloride density gradients, followed by dialysis in water and PBS. Endotoxins were removed by passages through an EndoTrap HD™ column (Hyglos, Germany) three times. Endotoxin levels were measured using the Endonext™ kit (Biomerieux) and a microplate fluorimeter (Tecan). The endotoxin level measured for the purified suspension was 10.05 EU/mL.

Bacteria from lung homogenates were enumerated by plating on cetrimide +1% glycerol agar plates (Sigma-Aldrich) and incubated overnight in 37 °C. Phage was enumerated by spotting serial dilutions on LB agar plates that were previously inundated by a fresh culture of PAKlumi and dried under a safety cabinet 30 min before use.

### Macrophage depletion
AM depletion was obtained by the intra-tracheal administration a single dose of 400 μg of clodronate liposomes or empty liposomes (LIPOSOMA, city), four days prior infection. For the intra-tracheal administration, the mice were anesthetized by intraperitoneal

injection of a mixture of two vol of ketamine (10 mg/mL) and one vol of xylazine (1 mg/mL) in a solution of NaCl 0.9%. The dose administered to each mouse was adjusted to 0.01 mg of the ketamine-xylazine mixture per 1 g of body mass.

## Flow cytometry analysis

To measure levels of AMs and PMNs three to four mice (receiving clodronate or empty lyposomes) were sacrificed and bronchoalveolar lavages (BALs) were obtained following Daubeaf et al.[48]. Briefly, we made an incision in the trachea, inserted a 22 G catheter (BD) and washed the lungs 3 times with 1 mL buffer with 2 % Fetal Bovine serum (Dulbcco's Phosphate Buffered Saline; STEMCELL), using a 1 mL syringe (BD). Cells from broncho-alveolar lavages were filtered through a 40 mm nylon mesh and first stained with a fixable live/dead marker for 30 min at room temperature (RT). Cells were washed with Cell Staining Buffer (BioLegend) and stained with a cocktail of surface antibodies for 20 min at 4 °C. Antibodies conjugated to various fluorochromes were used against the following mouse antigens: CD11b, CD11c, CD19, CD45, MHC II, Ly6C, Ly6G, F4/80, and TCRb. Cells were washed and then resuspended in 400 mL Cell Staining Buffer. Stained cells were analyzed using the ID7000 spectral cytometer (Sony). In every experiment single-stained samples in Ultracomp eBeads (Thermo Fisher), for each individual fluorochrome, were used as control. Data were analyzed using FlowJo software (BD).

## Estimating depletion effect of clodronate

We used the following model to represent clodronate pharmacokinetics and its effect on AM:

$$\dot{C} = -k_e C \qquad (1)$$

$$\dot{M}_A = \alpha_M M_A \left(1 - \frac{M_A}{M_m}\right) - k_{out_M} M_A \left(1 + \frac{E_{m,c}C}{C + C_{50}}\right) \qquad (2)$$

Where $C$ (Eq.(1)) is the clodronate amount in the lung, $k_e$ is the clodronate elimination rate from the lung, $M_A$ (Eq.(2)) is the AM concentration, $\alpha_M$ the self-renewal rate of macrophages, $M_m$ the maximal concentration of macrophages, $k_{out_M}$ the elimination rate of macrophages, $E_{m,C}$ the maximal effect of clodronate and $C_{50}$ the clodronate amount to reach 50% of the maximal effect. The initial condition of $C$ is given by the intratracheal dose of clodronate. The initial condition of $M_A$ is given by the data from uninfected, untreated and non-depleted mice, assuming the empty liposomes did not affect the alveolar macrophage level 96 h after administration.

## Murine model of acute pneumonia

Mice were first anesthetized by intraperitoneal injection of the same mixture of ketamine and xylazine as described above at a dose of 0.008 mg per 1 g of body mass. An exponentially growing culture of PAKlumi was washed three times in PBS before its density was adjusted to $1.25 \times 10^8$/mL in PBS. Mice were infected with a single intranasal administration of 40 µL ($5 \times 10^6$ CFU). Phage treatment was administered intranasally at a dose of $5 \times 10^7$ plaque forming units (PFU; MOI 10) in 40 µL PBS at 2 h p.i. The progression of infection was monitored by measuring the luminescence (IVIS, Perkin Elmer) produced by the bacteria from the lungs area of mice that were anesthetized by isoflurane inhalation. The LivingImage software (version 4.7.3; Xenogen)[14,34] was used to collect emitted photons within a consistent square ROI (2.5 by 3.0 cm), corresponding to the size and localization of the lungs. At end points lungs were collected and kept on ice in C tubes (gentleMACs™, Miltenyi Biotec) containing 1 mL PBS before homogenization with a tissue dissociator (Oligo-Macs, Miltenyi Biotec). The samples were serially diluted and plated on cetrimide agar.

## Conversion of bioluminescence data into bacterial load in lungs

We established the correlation between bioluminescence and CFU count using data from PAKlumi-infected and untreated animals for which emitted photons were recorded before lungs were taken, homogenized and plated to count bacteria (Supplementary Fig. 3). The relationship obtained allowed us to derive from the luminescence signal an equivalent counts of CFU per mL of lung (noted CFUeq/mL) that was used to obtain the bacterial loads in all infected animals (untreated or treated by phages) over time.

## Estimating in vivo AM-associated phage decay

Two groups of uninfected mice (AM-depleted and EL control) received a single dose of $5 \times 10^7$ PFU of phage PAK_P1 administered intranasally. At 24, 48, 72, and 96 h after phage administration, mice were sacrificed lungs were recovered, homogenized, and phages counts were measured as described above.

The phage decay was described using a monoexponential decay in AM-depleted mice (Eq.(3)):

$$\dot{P} = -\omega P \qquad (3)$$

where $\omega$ is the decay rate, which was estimated from uninfected and AM-depleted mice to obtain the decay of the phage PAK_P1 in absence of macrophages (assuming that the residual amount of macrophages was negligible). As the initial dose of phage ($d_P$, in PFU) was known and the initial phage concentration was given by the fit, the scaling factor (or distribution volume) $f_P$ was estimated, with the initial condition given as $P(0) = d_P/f_P$. The phage decay rate was augmented as follows by interactions with AM (Eq. 4):

$$\dot{P} = -\omega P - \psi P M_A. \qquad (4)$$

The AM-associated decay rate parameter $\psi$ was estimated from uninfected and control (empty liposome) mice, with $\omega$ fixed from experiments with AM-depleted mice. The AM level ($M_A$) was considered as stable during all experiments in the control group. Estimations were performed by naïve pooling of data (i.e., considering all the measures for each group (with or without clodronate) as if they came from a single individual and performing a non-linear regression, Fig. 2B).

## Quantification of phage DNA from AM-sorted from bronco-alveolar lavages

Anesthetized mice (see above) were intranasally administered with either a single dose of $5 \times 10^7$ PFU of phage PAK_P1 or PBS (40 µL). Four hours later, mice were euthanized, and bronchoalveolar lavage (BAL) was conducted according to Busch et al.[49]. Lavage was performed using 10 times 1 mL (total volume = 10 mL) of D-PBS containing 2% FBS (STEMCELL) and 2 mM EDTA (Invitrogen), which was pre-heated to 37 °C. A volume of 40 µL of BALs was taken to measure the number of viable phages while the rest was centrifuged at 500 g for 10 min at 4 °C, and the supernatant was discarded to remove free phage particles. The cells were then resuspended in hemolysis buffer (Biolegend) for 5 min at room temperature to lyse erythrocytes, followed by another centrifugation step (which correspond to a washing step to remove further any remaining free phage particles). Subsequently, cells were stained with antibodies against CD45 (BD), CD11c (Miltenyi Biotec), and Singlec-F (BD) (diluted 1:200) for 20 min in the dark at room temperature. After addition of 500 µL of D-PBS, AM were identified as positive for all three markers and sorted using the FACSAria III cell sorter (BD) in to 1 mL. Then 2 µL of each sample was used as template for a qPCR reaction with 450 nM of each primer (F-ACGCCA-GACCGAAGACAACT and R-CGTTCCAATCTCCCGCAACG) targeting the terminase large subunit (Gene ID: 10351274) using the PowerSYBR Green PCR master mix (Applied Biosystems) in a final volume of 15 µL

and run on BioRAD CFX Opus 96 Real-Time PCR System (denaturation step at 95 °C for 20 min followed by 40 cycles of amplification with denaturation at 95 °C for 10 s and annealing/elongation at 55 °C for 60 s). Fluorescence (FAM; Ex/Em 465/510 nm) was measured at the end of each cycle, and melting curve analysis was conducted to verify the specificity of the amplified PCR product. The number of DNA copies in each reaction was determined by comparing the Cycle threshold (Ct) to that of a sample with a known DNA concentration using a standard curve. Genomic DNA for standard curves was extracted using the Wizard Plus DNA purification system (Promega). DNA concentrations in ng/mL were measured by absorbance at 260 nm using a spectrometer (Eppendorf) and converted to gene copies/mL by inputting the genome length and concentration into the Technology Network Copy Number Calculator (https://www.technologynetworks.com/tn/tools/copynumbercalculator) for precise determination of copy numbers. The number of gene copies/mL was divided by the number of AM/mL sorted.

## Phage decay assessment in presence of J774 macrophages

Macrophage cell line J774.A1 (American Type Culture Collection No. TIB67) derived from BALB/c mice was maintained in RPMI 1640 medium + Glutamax™ (Gibco, Life Technologies Corporation, Grand Island, USA) and supplemented with 10 % (v/v) fetal calf serum (Eurobio scientific, Les Ulis, France). Cells were seeded at a density of $2 \times 10^5$ cells per well in 24-well tissue culture plates and grown for 18 h at 37 °C in an atmosphere enriched with 5% $CO_2$. Phage PAK_P1 was added to J774 monolayers or RPMI medium (control wells) at different phage:cells ratios ranging from 1:1 to 1000:1. At several times points (0, 1 h, 2 h, 4 h, 6 h and 24 h) supernatants were collected and phage titration performed as described above.

## Phagocytosis assay of phage PAK_P1 in presence of AM

BALs from 10 uninfected mice were collected according to Busch et al.[49]. Lavages were performed using 5 times 1 mL (total volume = 5 mL) of D-PBS containing 2% FBS (STEMCELL) and 2 mM EDTA (Invitrogen), which was pre-heated to 37 °C. The cells were then filtered through a 70 μm cell strainer and collected by centrifugation (400 g, 5 min, room temperature). Next, 1 ml of red blood cell lysis buffer (BioLegend) was added, followed by a 5-min incubation at room temperature. The lysis was stopped by adding 5 mL of complete medium (RPMI 1640, 1X GlutaMax, 10% FBS, 1X PenStrep, 1X sodium pyruvate) and cells were collected following a centrifugation (400 g, 5 min, room temperature) and resuspended in a total volume of 10 mL of complete medium. AMs (300 μL) were then distributed in chambers (Lab-Tek II Chamber Slide 8-wells, ThermoFisher) and incubated with or without 20 μM Cytochalasin B (C2743-200UL, Sigma-Aldrich) for 30 min at 37 °C. Phage PAK_P1 or beads (0.2 μm FluoSpheres™ Sulfate-Modified Yellow-Green Microspheres, Invitrogen #F8848) were added at a ratio of approximately 1000 phages or beads per AM. After 1, 3 and 5 h of incubation at 37 °C 4% PFA was added and "slides" were kept overnight at 37 °C. To detect phage particles a guinea pig primary antibody raised against phage PAK_P1 (Covalab) was applied (1/100 dilution), followed by a secondary antibody (anti-guinea pig Alexa Fluor 488, Abcam 150185, 1/500 dilution). The cytoplasm was stained with the CellMask membrane stain (C10046 ThermoFisher, 1/10,000), actin was labeled with Phalloidin 546 (A-30106 ThermoFisher, 1/750), and the nucleus was stained with DAPI (D1306 ThermoFisher, 1/8,000). Images were acquired on IX81 inverted microscope. A set of $n = 13$ to 47 macrophages per condition were randomly selected and analyzed (see Supplementary Methods and Supplementary Fig. 6).

## Model building, parameter estimation and model evaluation

The final mathematical model described in detail in Supplementary Methods was built following a sequential approach using the estimated parameters of clodronate effect on macrophages from the uninfected untreated mice and the macrophage effect on phage decay from the uninfected phage-treated mice. Key parameters of phage-immune cells-bacteria interactions were estimated from all the infected mice (AM-depleted and control, phage-treated and untreated). Inference procedures were performed in a non-linear mixed effect model framework using the SAEM algorithm implemented in Monolix software version 2021R2[50]. The individual parameters $\theta_i$ (with i the individual) followed a log Normal distribution ($\theta_i = \mu \exp(\eta_i)$, with $\mu$ the median parameter and $\eta_i$ the random effect for $i$, $\eta_i$ following a Normal distribution of expectancy 0 and standard deviation $\omega_i$). All inference procedures assumed an additive Gaussian error model on the log-transformed (bacteria and phage) data and a proportional error model on neutrophils (lung and blood), monocytes and macrophage data. The details of the choice and precision of estimation of parameter values (data used for estimation or reference in case of fixed parameter from the literature) are given in Table S1. The model selection was based on Bayesian information criterion[51]. Individual fits and residuals were investigated to evaluate the different models. The final model was also evaluated using normalized prediction distribution errors[36]. Graphic representations and simulations from the model and estimates were made with R using the RsSimulx package (version 2.0.2).

## Statistical analysis

Statistical analyses were performed using the Prism software (GraphPad, v9.5.0). Group comparisons were done using the Mann Whitney U test (independent samples), or the Wilcoxon sign test (paired samples). Log-rank (Mantel-Cox) test was used to compare survival curves. Pearson r correlation and simple line regression were used for correlation and dependency assessments.

## Reporting summary

Further information on research design is available in the Nature Portfolio Reporting Summary linked to this article.

## Data availability

The source data generated in this study has been deposited in the public database: https://doi.org/10.57745/M7T4ZJ.

## Code availability

The source code for the mathematical model is included in the Supplementary Information file and is available in GitFront: https://gitfront.io/r/jeremyseurat/c5QMQsU2Kjj3/MacrophagePhage/.

## References

1. WHO, O. (2017). One health. World Health Organ.
2. Bengtsson-Palme, J., Kristiansson, E. & Larsson, D. G. J. Environmental factors influencing the development and spread of antibiotic resistance. *FEMS Microbiol. Rev.* **42**, fux053 (2018).
3. Urban-Chmiel, R. et al. Antibiotic resistance in bacteria—A review. *Antibiotics* 11. https://doi.org/10.3390/antibiotics11081079 (2022).
4. Murray, C. J. L. et al. Global burden of bacterial antimicrobial resistance in 2019: a systematic analysis. *Lancet* **399**, 629–655 (2022).
5. Nikaido, H. Multidrug resistance in bacteria. *Annu. Rev. Biochem.* **78**, 119–146 (2009).
6. Gordillo Altamirano, F. L. & Barr, J. J. Phage therapy in the post-antibiotic era. *Clin. Microbiol. Rev.* **32**, e00066–18 (2019).
7. Hatfull, G. F., Dedrick, R. M. & Schooley, R. T. Phage therapy for antibiotic-resistant bacterial infections. *Annu. Rev. Med.* https://doi.org/10.1146/annurev-med-080219-122208 (2021).
8. Gómez-Ochoa, S. A. et al. Efficacy of phage therapy in preclinical models of bacterial infection: a systematic review and meta-analysis. *Lancet Microbe* **3**, e956–e968 (2022).
9. McCallin, S., Sacher, J. C., Zheng, J. & Chan, B. K. Current state of compassionate phage therapy. *Viruses* **11**, 343 (2019).

10. Pirnay, J.-P. et al. Retrospective, observational analysis of the first one hundred consecutive cases of personalized bacteriophage therapy of difficult-to-treat infections facilitated by a Belgian consortium. medRxiv. https://doi.org/10.1101/2023.08.28.23294728 (2023).

11. Zimecki, M. et al. Effects of prophylactic administration of bacteriophages to immunosuppressed mice infected with Staphylococcus aureus. *BMC Microbiol.* **9**, 169 (2009).

12. Green, S. et al. Bacteriophages from ExPEC reservoirs kill pandemic multidrug-resistant strains of clonal group ST131 in animal models of bacteremia. *Sci. Rep.* **7**, 46151 (2017).

13. Tiwari, B. R., Kim, S., Rahman, M. & Kim, J. Antibacterial efficacy of lytic Pseudomonas bacteriophage in normal and neutropenic mice models. *J. Microbiol. Seoul. Korea* **49**, 994–999 (2011).

14. Roach, D. R. et al. Synergy between the host immune system and bacteriophage is essential for successful phage therapy against an acute respiratory pathogen. *Cell Host Microbe* **22**, 38–47.e4 (2017).

15. Cairns, B. J., Timms, A. R., Jansen, V. A. A., Connerton, I. F. & Payne, R. J. H. Quantitative models of in vitro bacteriophage–host dynamics and their application to phage therapy. *PLOS Pathog.* **5**, e1000253 (2009).

16. Leung, C. Y. J. & Weitz, J. S. Modeling the synergistic elimination of bacteria by phage and the innate immune system. *J. Theor. Biol.* **429**, 241–252 (2017).

17. Marchi, J., Zborowsky, S., Debarbieux, L. & Weitz, J. S. The dynamic interplay of bacteriophage, bacteria and the mammalian host during phage therapy. *iScience* **26**, 106004 (2023).

18. Delattre, R. et al. Combination of in vivo phage therapy data with in silico model highlights key parameters for pneumonia treatment efficacy. *Cell Rep.* **39**, 110825 (2022).

19. Pardo, A. et al. Increase of Lung Neutrophils in Hypersensitivity Pneumonitis Is Associated with Lung Fibrosis. *Am. J. Respir. Crit. Care Med.* **161**, 1698–1704 (2000).

20. Cheng, P., Li, S. & Chen, H. Macrophages in lung injury, repair, and fibrosis. *Cells* 10. https://doi.org/10.3390/cells10020436 (2021).

21. Berg, J. T., Lee, S. T., Thepen, T., Lee, C. Y. & Tsan, M. F. Depletion of alveolar macrophages by liposome-encapsulated dichloromethylene diphosphonate. *J. Appl. Physiol.* **74**, 2812–2819 (1993).

22. Martin, T. R. & Frevert, C. W. Innate immunity in the lungs. *Proc. Am. Thorac. Soc.* **2**, 403–411 (2005).

23. Barletta, K. E. et al. Leukocyte compartments in the mouse lung: Distinguishing between marginated, interstitial, and alveolar cells in response to injury. *J. Immunol. Methods* **375**, 100–110 (2012).

24. Johnston, L. K., Rims, C. R., Gill, S. E., McGuire, J. K. & Manicone, A. M. Pulmonary Macrophage Subpopulations in the Induction and Resolution of Acute Lung Injury. *Am. J. Respir. Cell Mol. Biol.* **47**, 417–426 (2012).

25. Hou, F., Xiao, K., Tang, L. & Xie, L. Diversity of macrophages in lung homeostasis and diseases. *Front. Immunol.* **12**, 753940 (2021).

26. Raoust, E. et al. Pseudomonas aeruginosa LPS or flagellin are sufficient to activate TLR-dependent signaling in murine alveolar macrophages and airway epithelial cells. *PLOS ONE* **4**, e7259 (2009).

27. Lavoie, E. G., Wangdi, T. & Kazmierczak, B. I. Innate immune responses to Pseudomonas aeruginosa infection. *Microbes Infect.* **13**, 1133–1145 (2011).

28. Mijares, L. A. et al. Airway epithelial MyD88 restores control of Pseudomonas aeruginosa murine infection via an IL-1–dependent pathway. *J. Immunol.* **186**, 7080–7088 (2011).

29. Kooguchi, K. et al. Role of alveolar macrophages in initiation and regulation of inflammation in pseudomonas aeruginosapneumonia. *Infect. Immun.* **66**, 3164–3169 (1998).

30. Cheung, D. O. Y., Halsey, K. & Speert, D. P. Role of pulmonary alveolar macrophages in defense of the lung against pseudomonas aeruginosa. *Infect. Immun.* **68**, 4585–4592 (2000).

31. Koh, A., Priebe, G., Ray, C., Van Rooijen, N. & Pier, G. Inescapable need for neutrophils as mediators of cellular innate immunity to acute pseudomonas aeruginosa pneumonia. *Infect. Immun.* **77**, 5300–5310 (2009).

32. Jończyk-Matysiak, E. et al. Phage-phagocyte interactions and their implications for phage application as therapeutics. *Viruses* 9. https://doi.org/10.3390/v9060150 (2017).

33. Van Belleghem, J. D., Dąbrowska, K., Vaneechoutte, M., Barr, J. J. & Bollyky, P. L. Interactions between bacteriophage, bacteria, and the mammalian immune system. *Viruses* **11**, https://doi.org/10.3390/v11010010 (2018).

34. Debarbieux, L. et al. Bacteriophages can treat and prevent pseudomonas aeruginosa lung infections. *J. Infect. Dis.* **201**, 1096–1104. https://doi.org/10.1086/651135 (2010).

35. van Rooijen, N., Hendrikx, E. Liposomes for specific depletion of macrophages from organs and tissues. In Liposomes: Methods and Protocols, Volume 1: Pharmaceutical Nanocarriers, V. Weissig, ed. (Humana Press), pp. 189–203. https://doi.org/10.1007/978-1-60327-360-2_13 (2010).

36. Brendel, K., Comets, E., Laffont, C. & Mentré, F. Evaluation of different tests based on observations for external model evaluation of population analyses. *J. Pharmacokinet. Pharmacodyn.* **37**, 49–65 (2010).

37. Blériot, C., Ng, L. G. & Ginhoux, F. Cloaking" on time: A cover-up act by resident tissue macrophages. *Cell* **177**, 514–516 (2019).

38. Uderhardt, S., Martins, A. J., Tsang, J. S., Lämmermann, T. & Germain, R. N. Resident macrophages cloak tissue microlesions to prevent neutrophil-driven inflammatory damage. *Cell* **177**, 541–555.e17 (2019).

39. Shapouri-Moghaddam, A. et al. Macrophage plasticity, polarization, and function in health and disease. *J. Cell. Physiol.* **233**, 6425–6440 (2018).

40. Rubins, J. B. Alveolar Macrophages. *Am. J. Respir. Crit. Care Med.* **167**, 103–104 (2003).

41. Levy, B. D. & Serhan, C. N. Resolution of acute inflammation in the lung. *Annu. Rev. Physiol.* **76**, 467–492 (2014).

42. Wenger, S. L., Turner, J. H. & Petricciani, J. C. The cytogenetic, proliferative and viability effects of four bacteriophages on human lymphocytes. *Vitro* **14**, 543–549 (1978).

43. Barfoot, R. et al. Some properties of dendritic macrophages from peripheral lymph. *Immunology* **68**, 233–239 (1989).

44. Hodyra-Stefaniak, K. et al. Mammalian host-versus-phage immune response determines phage fate in vivo. *Sci. Rep.* **5**, 14802 (2015).

45. Lam, J., Herant, M., Dembo, M. & Heinrich, V. Baseline mechanical characterization of J774 macrophages. *Biophys. J.* **96**, 248–254 (2009).

46. Moir, D. T., Di, M., Opperman, T., Schweizer, H. P. & Bowlin, T. L. A high-throughput, homogeneous, bioluminescent assay for pseudomonas aeruginosa gyrase inhibitors and other DNA-damaging agents. *SLAS Discov.* **12**, 855–864 (2007).

47. Henry, M., Lavigne, R. & Debarbieux, L. Predicting in vivo efficacy of therapeutic bacteriophages used to treat pulmonary infections. *Antimicrob. Agents Chemother.* **57**, 5961–5968 (2013).

48. Daubeuf, F. & Frossard, N. Performing bronchoalveolar lavage in the mouse. *Curr. Protoc. Mouse Biol.* **2**, 167–175 (2012).

49. Busch, C. J.-L., Favret, J., Geirsdóttir, L., Molawi, K. & Sieweke, M. H. Isolation and long-term cultivation of mouse alveolar macrophages. *Bio-Protoc.* **9**, e3302 (2019).

50. Kuhn, E. & Lavielle, M. Maximum likelihood estimation in nonlinear mixed effects models. *Comput. Stat. Data Anal.* **49**, 1020–1038 (2005).

51. Delattre, M., Lavielle, M. & Poursat, M.-A. A note on BIC in mixed-effects models. *Electron. J. Stat.* **8**, 456–475 (2014).

## Acknowledgements

## Author contributions

## Competing interests

The authors declare no competing interests.

## Additional information

**Supplementary information** The online version contains supplementary material available at https://doi.org/10.1038/s41467-025-61268-1.

**Correspondence** and requests for materials should be addressed to Joshua S. Weitz or Laurent Debarbieux.

**Peer review information** *Nature Communications* thanks Rob de Boer, Antonia Sagona, and the other, anonymous, reviewers for their contribution to the peer review of this work. A peer review file is available.

**Reprints and permissions information** is available at http://www.nature.com/reprints

**Publisher's note** Springer Nature remains neutral with regard to jurisdictional claims in published maps and institutional affiliations.